AGU PUBLICATIONS

Geophysical Research Letters

RESEARCH LETTER
10.1002/2016GL068546

Key Points:
- First observation of frequency dependence of directivity effect in data from small earthquakes
- The directivity effect above the source corner frequency diminishes with increasing frequency
- Our observations suggest significant rupture-propagation complexity even for small earthquakes

Supporting Information:
- Supporting Information S1

Correspondence to:
F. Pacor,
francesca.pacor@ingv.it

Citation:
Pacor, F., F. Gallovič, R. Puglia, L. Luzi, and M. D'Amico (2016), Diminishing high-frequency directivity due to a source effect: Empirical evidence from small earthquakes in the Abruzzo region, Italy, *Geophys. Res. Lett.*, *43*, 5000–5008, doi:10.1002/2016GL068546.

Received 5 MAR 2016
Accepted 10 MAY 2016
Accepted article online 13 MAY 2016
Published online 27 MAY 2016

©2016. American Geophysical Union. All Rights Reserved.

Diminishing high-frequency directivity due to a source effect: Empirical evidence from small earthquakes in the Abruzzo region, Italy

F. Pacor[1], F. Gallovič[2], R. Puglia[1], L. Luzi[1], and M. D'Amico[1]

[1]Istituto Nazionale di Geofisica e Vulcanologia, Milan, Italy, [2]Department of Geophysics, Faculty of Mathematics and Physics, Charles University in Prague, Prague, Czech Republic

Abstract The aim of this study is to investigate the directivity effects of ~250 aftershocks (magnitudes 3–5.5) of the M_w 6.1 2009 L'Aquila earthquake (central Italy). To this end, we estimate the apparent source spectra at each station removing path and site effects inferred by standard Generalized Inversion Technique. Then, we evaluate the residuals between the apparent source spectra and the event mean source spectrum at selected frequencies. We investigate azimuthal and frequency dependence of the residuals for 40 events with the best station coverage. For most of events with the strongest directivity effect (M_w 3.4–4.0), we observe a remarkable decrease of the directivity amplification at high frequencies, which has not yet been documented for such relatively small-magnitude events. Since there is negligible distance dependence, we ascribe this observation to a source phenomenon such as significant small-scale rupture propagation complexity.

1. Introduction

Earthquake-source directivity effect is one of the key factors that affects ground shaking. Well-known examples are the two recordings of the M_w 7.3 1993 Landers earthquake (predominantly unilateral rupture propagation) at Lucerne and Joshua Tree stations with clearly pronounced forward and backward directivity effect, respectively [*Bernard et al.*, 1996; *Somerville et al.*, 1997; *Pacor et al.*, 2005]. Recently, as a result of increasing in quantity and quality of seismic observations, the directivity effect has been also recognized for small earthquakes [*Boatwright*, 2007; *Courboulex et al.*, 2013; *Calderoni et al.*, 2015]. Figure 1a shows records of an aftershock of the M_w 6.1 L'Aquila seismic sequence (03 May 2009, 05:14:45 *M*l3.2) at two rock sites, located at the same epicentral distance but in opposite direction with respect to the epicenter. These are clear examples of strong induced directivity amplification for a small earthquake. Since this directivity-amplification can be as large as one order, proper understanding of this effect is of utmost importance for seismic hazard assessment and earthquake engineering applications.

Directivity is similar to the Doppler effect as the rupture propagating along the fault, at velocity close to the shear wave speed, acts as a moving source. One consequence is a shift of the corner frequency (apparent corner frequency, f_a) and amplification/deamplification of source spectral amplitudes (apparent spectra), causing an azimuthal dependence of ground-shaking intensity with the maximum when the site is located in the forward direction with respect to the rupture propagation.

In case of a unilateral rupture propagating along a narrow fault at a constant velocity (linear Haskell model, *Haskell* [1964]), the change in corner frequency f_c can be parameterized by $f_a = f_c C_d(\theta)$, where $C_d(\theta)$ is the directivity coefficient [*Ben-Menahem*, 1961]:

$$C_d(\theta) = 1/(1 - \alpha\cos(\theta - \theta_r)) \quad (1)$$

In equation (1), $\alpha = v_r/c$ is the ratio between rupture velocity v_r and shear wave velocity c (also called Mach number), and θ and θ_r are the azimuths of the station and of the rupture direction, respectively.

While all theoretical source models agree on the proportionality between the corner frequency and C_d, the directivity amplification of the high-frequency acceleration spectrum above the corner frequency is still a subject of debate [e.g., *Ruiz et al.*, 2011]. The spectral ordinates scale proportionally to $C_d^n(\theta)$, where the exponent n depends on source model considered: omega-squared kinematic models with single corner frequency (e.g., *k*-squared model by *Herrero and Bernard* [1994]) suggest $n = 2$, while models with two corner frequencies (e.g., linear Haskell model with constant slip and risetime) suggest $n = 1$. More advanced models with

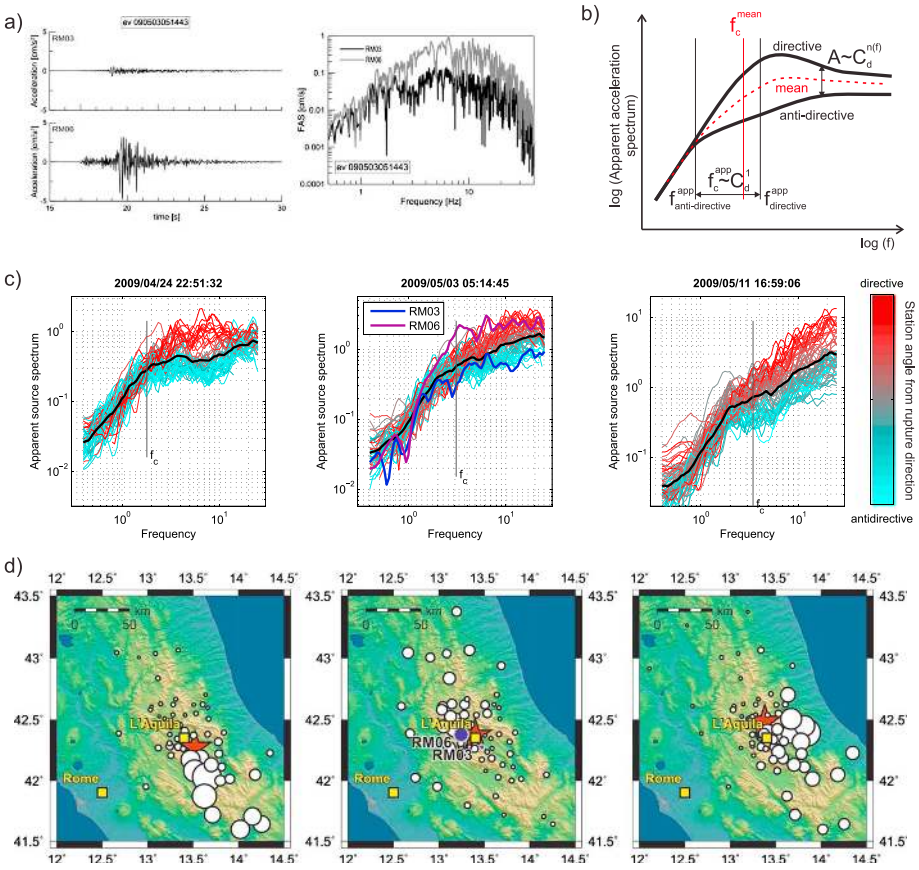

Figure 1. (a) Examples of acceleration waveforms recorded at rock stations, located approximately in the (top left) forward and (bottom left) backward directivity directions and (right) their Fourier spectra recorded at similar epicentral distances for one of the most directive events (03 May 2009, 05:14:45 *Ml* 3.2). (b) Schematic illustration of apparent source spectra described by the generalized *Ben-Menahem* [1961] directivity coefficient C_d^n (see equation (1)) with generally frequency-dependent *n* as suggested by advanced theoretical models (see text). We note that the mean spectrum (in red) is generally different from the apparent source spectrum of nondirective station due to the nonsymmetricity of the directivity function. (c) Apparent source spectra obtained after subtracting the site and path contributions from the observed spectra for the three selected events (for the other events see Figure S3); the color scale denotes the station angle from the direction of the rupture propagation; the black curves are the mean source spectra. The spectra relative to the 24 April 2009 event follow nicely the theoretical spectral shape illustrated in Figure 1b in the full frequency range, while the other two resemble only the increasing trend in its low-frequency part. (d) Spatial distribution of residuals (circles; their dimension is proportional to the residual amplitudes) at 7.06 Hz for events in Figure 1c. The stars denote hypocenters, the blue residuals in the middle plot correspond to RM01 and RM06 stations shown in Figure 1a.

inhomogeneous slip and risetime distributions or complex (incoherent) rupture propagation provide source radiation with frequency dependent *n*, typically decreasing from 2 or 1 to 0 in case of purely stochastic and composite models [*Zeng et al.*, 1994; *Bernard et al.*, 1996; *Pitarka et al.*, 2000; *Motazedian and Atkinson*, 2005; *Gallovič and Brokešová*, 2007; *Ruiz et al.*, 2011]. A sketch illustrating mean and apparent source spectra with *n* depending on frequency are reported in Figure 1b.

Earthquake source models with such decreasing *n* with increasing frequency have proven to be very successful in modeling strong motions due to large earthquakes. For example, *Gallovič* [2016] tested various directivity strengths using the source model by *Ruiz et al.* [2011], showing that the best fit with the observed near-fault strong motion data is provided by the model with the weakest high-frequency directivity (i.e., $n \sim 0.5$ for frequencies >1 Hz). Nevertheless, recordings of strongly directive large earthquakes are sparse, with a rather poor azimuthal station coverage not providing sufficient evidences to clarify this important

issue. In addition, wave propagation phenomena can mask the source directivity effect due to complex crustal properties along the path and/or close to the receivers.

Contrarily, the increasing availability of recordings of small events with good station coverage, due to the improvement of digital networks, has led to an increase of systematic studies on sources processes of such events. These studies show that the sources of small events can be complex as those of large earthquakes in terms of spatially variable slip and rupture propagation [*Dreger et al.*, 2007; *Kim et al.*, 2016]. The associated directivity effects are investigated analyzing the azimuthal dependence of the ground motions considering either peak values [*Boatwright*, 2007; *Cultrera et al.*, 2009] or duration of apparent source time functions [*Kane et al.*, 2013; *Courboulex et al.*, 2013; *Tan and Helmberger*, 2010]. *Chen et al.* [2014] considered the standard point-source model by *Brune* [1970], showing azimuthal variations of its corner frequency and approximately 2.5 higher spectral amplitudes at directive sites. *Tan and Helmberger* [2010] found evidence for directivity up to 7 Hz for events with magnitude lower than 5 in the 2003 M_w 5 Big Bear sequence. However, in those studies the authors have not investigated frequency dependence of the source directivity effect, which is the aim of our paper.

Here we exploit the study of *Pacor et al.* [2016], hereinafter denoted as PAC16, who applied the Generalized Inversion Technique (GIT) [*Andrews*, 1986; *Castro et al.*, 1990; *Prieto et al.*, 2004; *Shearer et al.*, 2006] to a very large high-quality data set of seismic records from small-to moderate events in central Italy. They investigated in detail the properties of the source spectra in this region and found evidence of forward directivity effects at stations located to the south-east of the epicenter for the M_w 6.1 main shock of the 2009 L'Aquila seismic sequence, in agreement with previous studies [*Ameri et al.*, 2012]. We extend the analysis of directivity to a large number of aftershocks using the results of the GIT as follows. We estimate the empirical source spectrum at each station (apparent source spectrum) by correcting the observed Fourier spectrum for the empirical attenuation and site terms. For each earthquake, we evaluate the residuals between the apparent source spectra and the event mean source spectrum and analyze them as a function of azimuth and frequency, which we interpret in terms of directivity models and rupture model complexity.

2. Description of the Data Set and Apparent Source Spectra Estimation

PAC16 collected a data set composed of more than 9000 accelerometric and velocimetric seismic records selected in central Italy, mainly composed of events of the 2009 L'Aquila seismic sequence (Figure S1 in the supporting information). This data set covers local magnitude range 3.0–5.8 and epicentral distances between 5 and 120 km (about 250 events and 130 stations). PAC16 analyzed this data set through the nonparametric GIT, as proposed by *Castro et al.* [1990] and *Oth et al.* [2008], to isolate frequency-dependent attenuation terms, source spectra, and site amplification functions. Following this inversion scheme, the individual terms are described nonparametrically, i.e., as general functions of frequency to avoid bias due to the use of too simplified spectral models fixed a priori.

PAC16 computed Fourier spectra of *S* wave time windows varying from 4 to 20 s in order to include a significant percentage of the total energy and smoothed the spectral amplitudes using the *Konno and Ohmachi* [1998] algorithm. The inversion was performed for the vector composition of the horizontal components at 73 frequencies equally spaced on a logarithmic scale in the range of 0.2–25 Hz. In this study, the nonparametric functions found by PAC16 are used to estimate the apparent source spectra as follows. For each frequency f, the observed spectral amplitudes $U(f,r)$ at hypocentral distance r, are described by the product of source $S(f)$, path $A(f,r)$, and site $G(f)$ in the form $U(f,r) = S(f)A(f,r)G(f)$. The apparent source spectrum Sa_{ij}, for each event i and station j, is then obtained removing the contribution of the empirical site and attenuation terms from the observed spectra, i.e., $Sa_{ij}(f,r) = U_{ij}(f,r)/[A_{ij}(f,r)G_j(f)]$.

Since our analysis of directivity effects needs an optimal azimuthal coverage, from the PAC16 data set we select a subset of events, which were recorded by at least 50 stations and with more than 5 stations in each quadrant. These criteria are satisfied by 40 out of the 250 events. Figure S2 shows the mean source spectra of these 40 events. They generally exhibit classical omega-squared shape with spectral plateau at high frequencies, although some of them exhibit either decay or increase with increasing frequency. PAC16 calculated the high-frequency decay parameter k through the fit to the *Anderson and Hough* [1984] model for frequencies higher than 10 Hz and found that the k values are normally distributed with mean value almost zero. This

means that the high-frequency trends are mainly included in the empirical attenuation and site terms and do not affect the mean source spectra. These results confirm that, on average, the mean source spectra of the investigated events have the omega-squared shape (Figure S2).

Figure 1c shows apparent source spectra and the nonparametric mean source spectrum for three selected events that exemplify the observed shapes of the most directive events of our data set (see further). The apparent source spectra do not generally attain the classical omega-squared shape. Indeed, such spectra are better predicted by theoretical models with frequency-dependent directivity amplification, as schematically illustrated in Figure 1b. In particular, the apparent spectra of event 24 April 2009, 22:51:32 (# 3 of Table S1 in the supporting information, Figure 1c, left), resemble the theoretical ones in Figure 1b having weakened directivity effect at high frequencies. Contrarily, the spectra of the third event in Figure 1c (#10 of Table S1), where the directivity effect remains strong at all frequencies, reproduce only the low-frequency part of the theoretical spectrum. Qualitatively, these two cases represent limiting cases for the apparent source spectra of other strongly directive events from our data set as shown in Figure 1c, middle (#6 of Table S1) and in Figure S3.

To quantify the frequency and azimuthal dependence of directivity, for each event we analyze the residuals defined as the difference between the apparent source spectra Sa_{ij} and the mean source spectrum S_i in the log domain. Figure 1d shows examples of the spatial distributions of the residuals for three earthquakes at 7 Hz. The residuals exhibit a clear azimuthal dependency variable from earthquake to earthquake. The event 03 May 2009 05:14:45 (event #6) of Figure 1d exhibits the largest residuals located NW of the epicenters, while the other two earthquakes have the largest residuals to SE (events # 3 and #10). In particular, the NW-SE direction agrees with the strike of the Apennines mountain chain (Figure 1d), where the main regional seismogenic fault system is recognized. It consists of both east dipping, prevailingly low-angle, and west dipping, prevailingly high-angle, normal fault systems. On the base of the examples shown in Figure 1, we suppose that the azimuthal dependence is related to source phenomena, since it cannot be ascribed to wave-propagation effects, such as anisotropy or regional amplification effects. The radiation pattern effect can be excluded as a cause of such trends since our analyses are carried out on the vector composition of horizontal spectral amplitudes. Moreover, several studies [e.g., *Liu and Helmberger*, 1985; *Takemura et al.*, 2009; *Kobayashi et al.*, 2015] show that azimuthal differences among seismograms, due to radiation pattern, diminish at high-frequencies (>3 Hz). In particular, *Kobayashi et al.* [2015] clearly demonstrate that for frequencies above 6 Hz the spatial pattern of maximum amplitudes is distorted from the expected four-lobe pattern even for *P* wave seismograms at distances less than 50 km. Finally, it is important to note that the residuals are almost independent of distance.

Figure 2 shows the distribution of residuals as a function of station azimuth at four frequencies for the three directive events of Figures 1c and 1d. A clear trend of the residuals can be recognized in most cases with a distinct maximum in correspondence of the azimuth of the rupture propagation. While the amplitudes of the trend are almost independent of hypocentral distance, they vary from event to event and also with frequency. These residual distributions represent a measure of the strength of the event-directivity and its frequency dependence, which is the main topic of the following analysis.

3. Analysis of the Source-Spectrum Residuals

The residuals between the apparent source spectrum and the event mean source spectrum are fitted by the following function for each frequency:

$$f(\theta) = \log_{10} C_d^n(\theta) - < \log_{10} C_d^n(\theta) > \quad (2)$$

where θ is the azimuth, the symbol $<>$ denotes the azimuthal average, and $C_d(\theta)$ is the directivity coefficient reported in equation (1). In equation (2) the unknown parameters are the azimuth of the rupture direction, θ_r; the ratio between rupture and *S* wave velocities, α; and the exponent *n*. As illustrated in Figure S4, the same fitting functions are obtained for various combinations of the latter two parameters, which results in a strong trade-off between α and *n*. Therefore, it is necessary to fix either of them.

Among the 40 events with good azimuthal coverage, we first identify those with the strongest directivity effects. To this end, we fit the residuals to equation (2) fixing *n* equal to 1, which means assuming the directivity coefficient of the linear Haskell model, as it is a standard used by other authors [*Boatwright*,

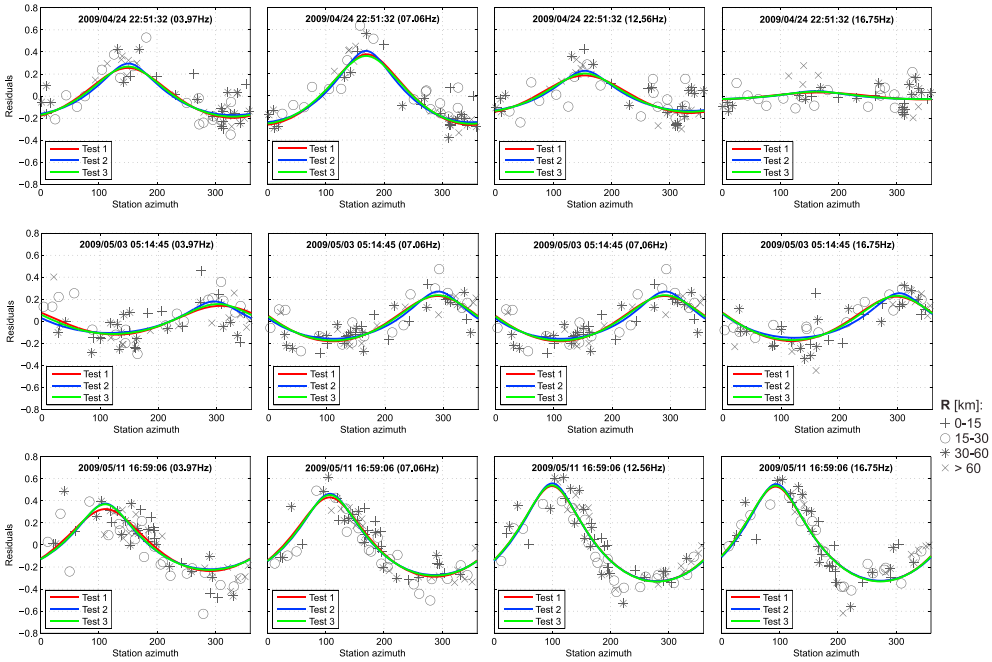

Figure 2. Residuals (symbols) for four frequencies (columns) and the three events (rows) of Figures 1c and 1d (for the other events see Figure S3). The various symbols reflect the station hypocentral distance range (see legend to the right), showing that the residuals have no or very weak distance dependence. The lines represent fitting of the residuals by the theoretical directivity function in equation (2), fixing either exponent n or rupture to S wave velocity ratio α (see legend and explanation of Tests 1–3 in the text). As a consequence of the trade-off between these parameters (as illustrated in Figure S4), the fit is almost exactly the same.

2007; *Tan and Helmberger*, 2010; *Kane et al.*, 2013; among others]. We seek for the direction of the rupture propagation θ_r and ratio α by means of least squares fitting (this analysis is termed Test 1). In this way, we implicitly assume only horizontal rupture propagation, where the signature of directivity as a function of angle is maximized. The fitting curves are shown in red in Figure 2. Note that the fitting curve reproduces the asymmetrical distribution of the residuals very well; that is, the peak in the forward directivity is narrower and with larger amplitude than the smoother minimum in the opposite direction.

To select the strongest directivity events (i.e., with predominantly unilateral horizontal rupture propagation) we apply the following criteria: (i) the root-mean-square error of $f(\theta)$, averaged in the frequency range ($2\,f_c - 5\,f_c$), is lower than or equal to 0.15 and (ii) $\alpha \geq 0.4$. Parameter α is considered here as an indicator of the strength of directivity: the larger is α, the larger is the amplitude of the peaks of the fitting function. The criteria are satisfied by 10 most directive events, which are summarized in Table S1 and plotted in Figure S1. These 10 earthquakes are strongly directive with a good spatial station coverage, providing us high degree of confidence in the investigation of the frequency dependence of directivity. The selection is more restrictive than the one adopted by *Calderoni et al.* [2015], who identified the directive events of the L'Aquila sequence applying a spectral ratio technique.

Figure 3 shows examples of the best fit parameters θ_r and α as a function of frequency for Test 1 (in red) and 6 (events #3, #6, #10, #8, #5, and #1) out of the 10 selected events (results for all the events are shown in Figure S3). The direction of the rupture propagation is stable at frequencies beyond the corner frequency and takes different values for the selected events, confirming the independence from other effects (e.g., anisotropy in wave propagation or regional site effects). The extreme stability of the azimuth of the rupture propagation is a valid support to the directivity hypothesis and confirms the robustness of the model used in this study, despite its simplicity.

On the other hand, α is very small up to the corner frequency, then increases to its maximum and eventually drops to small values (~0.2) at frequencies roughly larger than ~10 Hz. Only the event #10 (11 May 2009,

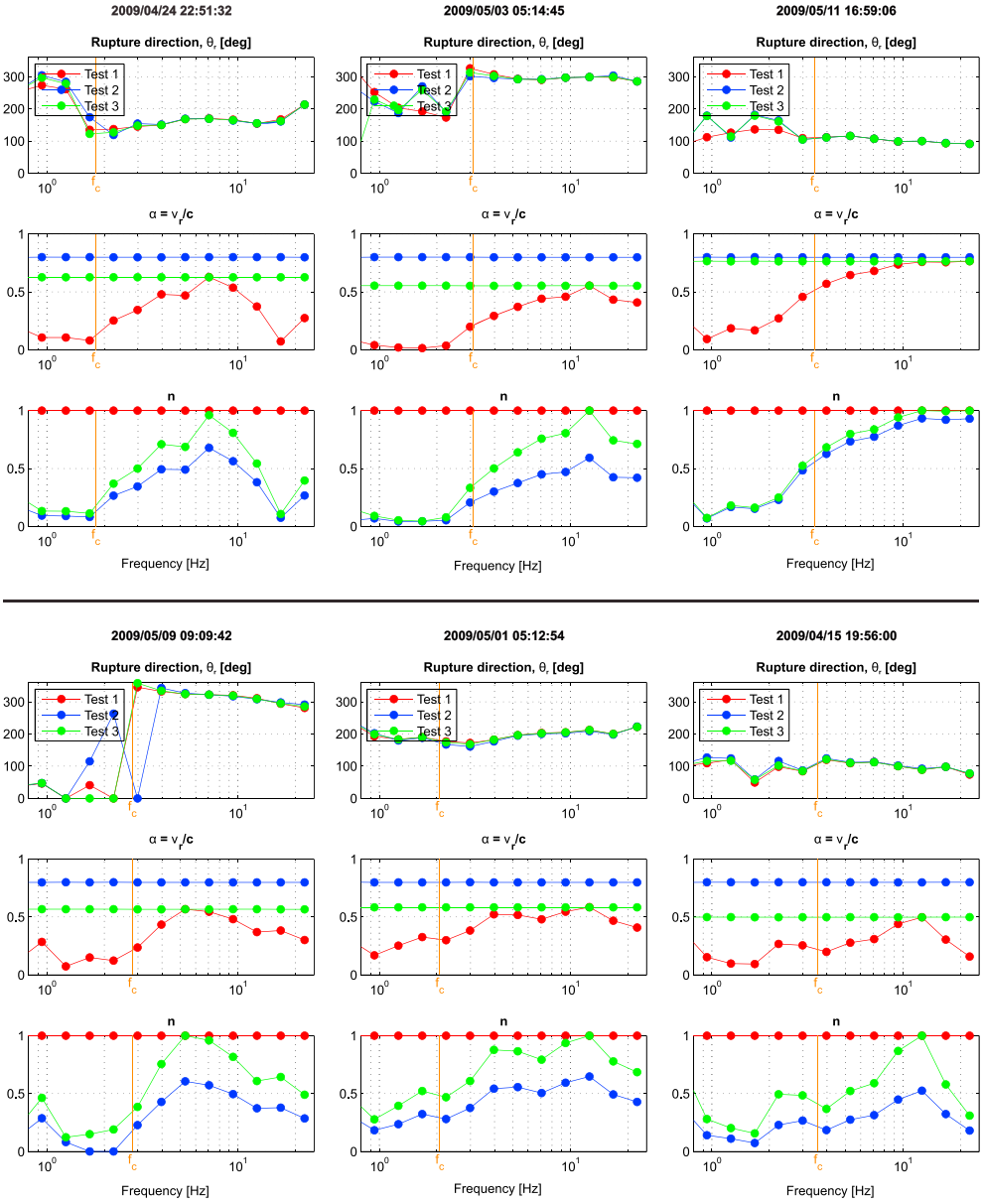

Figure 3. Inferred directivity parameters (top row) θ_r, (middle row) α, and (bottom row) n as a function of frequency for six selected events and Tests 1–3, see legend (for other events see Figure S3). Corner frequency f_c inferred by PAC16 is denoted by the orange vertical line. Note the stability of the inferred rupture directions above the corner frequencies. The small values of n or α are signatures of weak directivity effect because the fitting function flattens in such cases. The weak directivity happens not only below the corner frequency (where the source radiates as a point source) but also at high frequencies in most cases. Since the latter appears to be distance independent (see Figure 2), we ascribe it to diminishing high-frequency directivity effect due to a source effect.

16:59:06) is characterized by a rupture velocity approximately equal to 0.8 times the shear wave velocity, which is a typically accepted value, and remains constant up to the largest investigated frequency. All other events are characterized by smaller values of the maximum rupture velocities.

The dependence of α on frequency is not physical. However, it may be understood as a proxy to frequency dependence of some other source phenomenon. As an alternative, we investigate the frequency dependence of the directivity effect in terms of the exponent n in equation (2). Two additional tests are performed

on the 10 selected events: (i) Test 2: α is fixed to 0.8 independently on frequency (i.e., a value generally adopted for ground motion simulations), and the frequency dependence of n and θ_r is evaluated; (ii) Test 3: α is set to the maximum value obtained in Test 1, and the frequency dependence of n and θ_r is evaluated.

The results are summarized in Figure 3 (Test 2, in blue; Test 3, in green) for six sample events (the results for all events are in Figure S3). For both tests, exponent n exhibits the same frequency dependence as α in Test 1, while the amplitudes of n are shifted to compensate the difference between the adopted values for α (cf. blue and green curves in Figures 3 and S3).

As we pointed out in the introduction, the frequency dependence of n can be explained by advanced kinematic source models. Let us emphasize that in the three cases, the goodness of fit with the residuals is similar (Figure 2); therefore, we cannot determine, which of directivity models is more suitable to describe the observations. However, our findings provide clear evidence of the diminution of source directivity with increasing frequency, independently from the considered kinematic model, and the values assigned to the fixed parameters.

4. Discussion and Conclusions

Ground motions generated by unilateral rupture propagation are affected by directivity effects, described by functions depending on the station azimuth. These effects are persistent also in case of source model, in which the rupture propagates smoothly and the slip distribution is strongly heterogeneous. Some existing kinematic models propose frequency-dependent source directivity effects, assuming complex rupture propagation in terms of incoherence of rupture velocity and/or dependence of the risetime on the spatial scale (so-called k-dependent risetime). For example, widely used broadband simulations techniques [e.g., *Pitarka et al.*, 2000; *Gallovič and Brokešová*, 2007] generate high-frequency ground motion through composite source model implicitly considering no or very weak directivity effects [*Gallovič and Burjánek*, 2007]. Other kinematic models with strongly heterogeneous evolution of the rupture include varying direction of rupture propagation at small scales [*Herrero and Bernard*, 1994; *Ruiz et al.*, 2011; *Gusev*, 2014], thus destroying directivity effect at high frequency.

The aim of this paper is to provide empirical evidence of the frequency and azimuthal dependence of directivity from the analysis of small-to-moderate earthquakes. The investigated data set consists of accelerometric and velocimetric records from 250 aftershocks of the 2009 M_w 6.1 L'Aquila earthquake (central Italy). In this study we exploited the empirical nonparametric attenuation terms and the site amplification functions as inferred by *Pacor et al.* [2016] using a generalized spectral inversion applied to the same data set to compute the apparent source spectra at each station. For each record, we evaluated the residuals between the apparent source spectrum and the mean source spectrum of the corresponding event. By fitting the residuals through the Ben-Menahem directivity function $C_d(\theta)$, we identified the 10 most directive events present in the data set. The residuals of these events were then matched by the generalized directivity function $C_d^n(\theta)$ to evaluate the ratio α between rupture and S wave velocities, the azimuth θ_r of rupture propagation, and the exponent n for each event. Due to the strong trade-off between α and n we had to fix either of them to a constant value.

The main results can be summarized as follows:

1. Residuals exhibit a remarkable dependence on station azimuth and frequency. Since the azimuthal distributions of the residuals are independent of distance, we suppose that these features are mainly controlled by source processes.
2. The direction of rupture propagation θ_r is constant with frequency and in agreement with the NW-SE alignment of the Abruzzo fault systems.
3. Directivity models where the parameters α and n are frequency-dependent reproduce very well the observed azimuthal and frequency trends of the residuals. We speculate that this frequency dependence of the parameters α and n could be a proxy of rupture complexity at the corresponding wavelengths.
4. Independently of model used to fit the residuals, we observe that for most of the events the directivity function reaches its maximum above the source corner frequency and then decreases with frequency as predicted by the generalized directivity model (Figure 3). We interpret this decrease as an evidence that the directivity effect diminishes at high frequencies. We may also suppose that in case of persistent directivity effects, the observed spectra are incomplete due to the limited frequency range analyzed. This

means that such spectra could get flattened at frequencies higher than those investigated. For example, the apparent spectra of events 11 May 2009, 16:59:06 (event #10 of Table S1, Figure 1c, right) and 26 April 2009 17:56:08 (event #4 of Table S1 and Figure S3), which are characterized by the largest corner frequencies and stress drops, reproduce only the increasing trend of the theoretical model (Figure 1b).

This work documents that the weakening of the directivity effect (when present) starts roughly at ~10 Hz. Since the corner frequency of the analyzed events varies between 1.6 and 3.8 Hz, we speculate that rupture complexity becomes significant at scales smaller than ~1/5 of the source dimensions. We interpret this reduction of directivity at high frequencies as a consequence of rupture incoherence and/or scale dependence of risetime. We note that there are other studies supporting our findings. For example, complexity in source rupture process of small events was also identified by *Kim et al.* [2016] as one possible cause of the modification of radiation pattern of high-frequency *P* waves. Analogue experiments of *Day et al.* [2008] on simulating earthquake with unilateral rupture propagation in laboratory foam rubber show strong complexity in rupture propagation. They hypothesized that this complexity is generated by localized strong barriers that initially withstand the main rupture front arrival and break later with even significantly different rupture direction (see also laboratory experiments by *Latour et al.* [2013]). These barriers can also be represented by irregularities in the fault geometry [*Shi and Day*, 2013]. Such rupture propagation results in complex shape of slip rate functions along the fault, which adds up incoherence in the resulting radiated wavefield, distorting coherent rupture growth, and leading to directivity effect that decreases with increasing frequency.

Our evidences of frequency dependence of the directivity based on recordings of small events provide clues for better understanding the complexity of earthquake sources in terms of their small-scale rheological and/or geometrical features. We suppose that these findings can be extrapolated to larger events, where the weakening of directivity is typically related to complexity in wave propagation, such as scattering [e.g., *Imperatori and Mai*, 2012; *Sato et al.*, 2012] rather than in source process. This implies that the high-frequency directivity effect will be weak even at short distances, where the source contributions dominate the ground motions.

We point out that at such evidences from large earthquakes are hardly identifiable, due to insufficient number of near-fault data. The diminution of the high-frequency directivity would reduce the potential ground motion amplification due to the rupture propagation, with significant consequences for near fault seismic hazard assessment at short periods.

Acknowledgments
We thank Dino Bindi, Adrien Oth, and Daniele Spallarossa for their useful discussions; Chiara Felicetta for her help in preparing Figure S1. We are also grateful to F. Courboulex, A. Herrero and two anonymous reviewers for their constructed comments that helped to improve the manuscript. This work was financially supported by "FIRB—Abruzzo' Project (UR7) funded by Ministero dell'Istruzione dell'Università e della Ricerca and by the Czech Science Foundation project 14-04372S.

References

Ameri, G., F. Gallovič, and F. Pacor (2012), Complexity of the Mw 6.3 2009 L'Aquila (central Italy) earthquake: 2. Broadband strong motion modeling, *J. Geophys. Res.*, *117*, B04308, doi:10.1029/2011JB008729.

Anderson, J. G., and S. E. Hough (1984), A model for the shape of the Fourier amplitude spectrum of acceleration at high frequencies, *Bull. Seismol. Soc. Am.*, *74*, 1969–1993.

Andrews, D. J. (1986), Objective determination of source parameters and similarity of earthquakes of different size, in *Earthquake Source Mechanics*, edited by S. Das, J. Boatwright, and C. H. Scholz, AGU, Washington, D. C.

Ben-Menahem, A. (1961), Radiation of seismic surface waves from finite moving sources, *Bull. Seismol. Soc. Am.*, *51*, 401–435.

Bernard, P., A. Herrero, and C. Berge (1996), Modeling directivity of heterogeneous earthquake ruptures, *Bull. Seism. Soc. Am.*, *86*, 1149–1160.

Boatwright, J. (2007), The persistence of directivity in small earthquakes, *Bull. Seismol. Soc. Am.*, *97*(6), 1850–1861, doi:10.1785/0120050228.

Brune, J. N. (1970), Tectonic stress and the spectra of seismic shear waves from earthquakes, *J. Geophys. Res.*, *75*, 4997–5009.

Calderoni, G., A. Rovelli, Y. Ben-Zion, and R. Di Giovambattista (2015), Along-strike rupture directivity of earthquakes of the 2009 L'Aquila, central Italy, seismic sequence, 203, *Geophys. J. Int.*, *205*, 399–415, doi:10.1093/gji/ggv275.

Castro, R. R., J. G. Anderson, and S. K. Singh (1990), Site response, attenuation and source spectra of S waves along the Guerrero, Mexico, subduction zone, *Bull. Seismol. Soc. Am.*, *80*, 1481–1503.

Chen, Y., J. Letort, F. Cotton, and S. Drouet (2014), High-frequency directivity effects: Evidence from analysis of the Les Saintes records, *J. Seismol.*, *18*, 457–466.

Courboulex, F., A. Dujardin, M. Vallee, B. Delouis, C. Sira, A. Deschamps, L. Honore, and F. Thouvenot (2013), High-frequency directivity effect for an Mw 4.1 earthquake, widely felt by the population in southeastern France, *Bull. Seismol. Soc. Am.*, *103*, 3347–3353.

Cultrera, G., F. Pacor, G. Franceschina, and M. Cocco (2009), Directivity effects for moderate-magnitude earthquakes (Mw 5.6–6.0) during the 1997 Umbria-Marche sequence, central Italy, *Tectonophysics*, *476*, 110–120.

Day, S. M., S. H. Gonzalez, R. Anooshehpoor, and J. N. Brune (2008), Scale-model and numerical simulations of near-fault seismic directivity, *Bull. Seismol. Soc. Am.*, *98*(3), 1186–1206, doi:10.1785/0120070190.

Dreger, D. S., R. M. Nadeau, and A. Chung (2007), Repeating earthquake finite source models: Strong aspirates revealed on the San Andreas Fault, *Geophys. Res. Let.*, *34*, L23302, doi:10.1029/2007GL031353.

Gallovič, F. (2016), Modeling velocity recordings of the Mw6.0 South Napa, California, earthquake: Unilateral event with weak high-frequency directivity, *Seism. Res. Lett.*, *87*, 2–14.

Gallovič, F., and J. Brokešová (2007), Hybrid k-squared source model for strong ground motion simulations: Introduction, *Phys. Earth Planet. Inter.*, *160*, 34–50.

Gallovič, F., and J. Burjánek (2007), High-frequency directivity in strong ground motion modeling methods, *Ann. Geophys.*, *50*, 203–211.
Gusev, A. A. (2014), Doubly stochastic earthquake source model: "Omega-Square" spectrum and low high-frequency directivity revealed by numerical experiments, *Pure Appl. Geophys.*, *171*, 2581–2599.
Haskell, N. (1964), Total energy and energy spectral density of elastic wave radiation from propagating faults, *Bull. Seismol. Soc. Am.*, *54*, 1811–1851.
Herrero, A., and P. Bernard (1994), A kinematic self-similar rupture process for earthquakes, *Bull. Seism. Soc. Am.*, *84*, 1216–1228.
Imperatori, W., and M. P. Mai (2012), Broad-band near-field ground motion simulations in 3-dimensional scattering media, *Geophys. J. Int.*, *192*(2), 725–744.
Kane, D. L., P. M. Shearer, B. P. Goertz-Allmann, and F. L. Vernon (2013), Rupture directivity of small earthquakes at Parkfield, *J. Geophys. Res. Solid Earth*, *118*, 212–221, doi:10.1029/2012JB009675.
Kim, A., D. S. Dreger, T. Taira, and R. M. Nadeau (2016), Changes in repeating earthquake slip behavior following the 2004 Parkfiled main shock from waveform empirical Green's functions finite-source inversion, *J. Geophys. Res. Solid Earth*, *121*, 1910–1926, doi:10.1002/2015JB012562.
Kobayashi, M., S. Takemura, and K. Yoshimoto (2015), Frequency and distance changes in the apparent P-wave radiation pattern: Effects of seismic wave scattering in the crust inferred from dense seismic observations and numerical simulations, *Geophys. J. Int.*, *202*, 1895–1907, doi:10.1093/gji/ggv263.
Konno, K., and T. Ohmachi (1998), Ground-motion characteristics estimated from spectral ratio between horizontal and vertical components of microtremor, *Bull. Seism. Soc. Am.*, *88*, 228–241.
Latour, S., C. Voisin, F. Renard, E. Larose, S. Catheline, and M. Campillo (2013), Effect of fault heterogeneity on rupture dynamics: An experimental approach using ultrafast ultrasonic imaging, *J. Geophys. Res. Solid Earth*, *118*, 5888–5902, doi:10.1002/2013JB010231.
Liu, H., and D. V. Helmberger (1985), The 23:19 aftershock of the 15 October 1979 Imperial Valley earthquake: More evidence for an asperity, *Bull. Seismol. Soc. Am.*, *75*, 689–708.
Motazedian, D., and G. M. Atkinson (2005), Stochastic finite-fault modeling based on a dynamic corner frequency, *Bull. Seismol. Soc. Am.*, *95*, 995–1010.
Oth, A., D. Bindi, S. Parolai, and F. Wenzel (2008), S-wave attenuation characteristics beneath the Vrancea region in Romania: New insights from the inversion of ground-motion spectra, *Bull. Seismol. Soc. Am.*, *98*, 2482–2497.
Pacor, F., G. Cultrera, A. Mendez, and M. Cocco (2005), Finite fault modeling of strong ground motions using a hybrid deterministic-stochastic approach, *Bull. Seism. Soc. Am.*, *95*, 225–240.
Pacor, F., D. Spallarossa, A. Oth, L. Luzi, R. Puglia, L. Cantore, A. Mercuri, M. D'Amico, and D. Bindi (2016), Spectral models for ground motion prediction in the L'Aquila region (central Italy): Evidence for stress-drop dependence on magnitude and depth, *Geophys. J. Int.*, *204*, 697–718.
Pitarka, A., P. G. Somerville, Y. Fukushima, T. Uetake, and K. Irikura (2000), Simulation of near-fault ground motion using hybrid Green's functions, *Bull. Seismol. Soc. Am.*, *90*, 566–586.
Prieto, G., P. M. Shearer, F. L. Vernon, and D. Kilb (2004), Earthquake source scaling and self-similarity estimation from stacking P and S spectra, *J. Geophys. Res.*, *109*, B08310, doi:10.1029/2004JB003084.
Ruiz, J. A., D. Baumont, P. Bernard, and C. Berge-Thierry (2011), Modelling directivity of strong ground motion with a fractal, k-2, kinematic source model, *Geophys. J. Int.*, *186*, 226–244.
Shearer, P. M., G. A. Prieto, and E. Hauksson (2006), Comprehensive analysis of earthquake source spectra in southern California, *J. Geophys. Res.*, *111*, B06303, doi:10.1029/2005JB003979.
Shi, Z., and S. M. Day (2013), Rupture dynamics and ground motion from 3-D rough-fault simulations, *J. Geophys. Res. Solid Earth*, *118*, 1–20, doi:10.1002/jgrb.50094.
Somerville, P., N. F. Smith, W. Graves, and N. Abrahamson (1997), Modification of empirical strong ground motion attenuation relations to include the amplitude and duration effects of rupture directivity, *Seismol. Res. Lett.*, *68*, 199–222.
Takemura, S., T. Furumura, and T. Saito (2009), Distortion of the apparent S-wave radiation pattern in the high-frequency wavefield: Tottori-ken Seibu, Japan, earthquake of 2000, *Geophys. J. Int.*, *178*, 950–961, doi:10.1111/j.1365-246X.2009.04210.x.
Tan, Y., and D. Helmberger (2010), Rupture directivity characteristics of the 2003 Big Bear Sequence, *Bull. Seismol. Soc. Am.*, *100*, 1089–1106.
Sato, H., M. Fehler, and T. Maeda (2012), *Seismic Wave Propagation and Scattering in the Heterogeneous Earth Structure*, 2nd ed., Springer, Berlin, doi:10.1007/978-3-642-23029-5.
Zeng, Y., J. Anderson, and G. Yu (1994), A composite source model for computing realistic synthetic strong ground motions, *Geophys. Res. Lett.*, *21*, 725–728.